PNAS RESEARCH ARTICLE | PHYSIOLOGY OPEN ACCESS

cAMP and voltage modulate rat auditory mechanotransduction by decreasing the stiffness of gating springs

Andrew A. Mecca[a,b,1], Giusy A. Caprara[a,1], and Anthony W. Peng[a,2]

Edited by Robert Fettiplace, University of Wisconsin–Madison, Madison, WI; received April 21, 2021; accepted June 13, 2022

Hair cells of the auditory and vestibular systems transform mechanical input into electrical potentials through the mechanoelectrical transduction process (MET). Deflection of the mechanosensory hair bundle increases tension in the gating springs that open MET channels. Regulation of MET channel sensitivity contributes to the auditory system's precision, wide dynamic range and, potentially, protection from overexcitation. Modulating the stiffness of the gating spring modulates the sensitivity of the MET process. Here, we investigated the role of cyclic adenosine monophosphate (cAMP) in rat outer hair cell MET and found that cAMP up-regulation lowers the sensitivity of the channel in a manner consistent with decreasing gating spring stiffness. Direct measurements of the mechanical properties of the hair bundle confirmed a decrease in gating spring stiffness with cAMP up-regulation. In parallel, we found that prolonged depolarization mirrored the effects of cAMP. Finally, a limited number of experiments implicate that cAMP activates the exchange protein directly activated by cAMP to mediate the changes in MET sensitivity. These results reveal that cAMP signaling modulates gating spring stiffness to affect auditory sensitivity.

stereocilia | cyclic AMP | LDM | hair bundle mechanics | EPAC

Hair cells of the auditory and vestibular systems convert mechanical input from sound and head movement into an electrical current through a process termed mechanoelectrical transduction (MET). At the apical surface of each hair cell is a specialized mechanosensitive organelle called the hair bundle, composed of a collection of actin-filled stereocilia arranged in graded height. The tips of the shorter rows house MET channels (1), nonspecific cation channels hypothesized to be comprised of TMC1/2, TMIE, and a number of other accessory proteins (2–4). MET channels are gated by a tension force imparted by a gating spring, which is part of or connected with the filamentous tip links that span adjacent rows of stereocilia (5–9). Positive stimuli directed along the sensitive axis of the hair bundle (10) result in displacement toward the tallest row and increase tension in the gating spring, increasing the open probability of the MET channel.

Mechanisms that regulate the sensitivity of the MET channel are hypothesized to contribute to the wide dynamic range and frequency selectivity of the auditory system, with MET adaptation being the most widely studied (11–14). Based on the gating spring theory, changes in gating spring stiffness alter the setpoint and the sensitivity of the MET channel (5, 6). The second messenger cyclic adenosine monophosphate (cAMP) has been proposed to modulate the sensitivity of the MET channel in turtle and bullfrog hair cells. In turtle auditory hair cells, cAMP shifts the operating point of the MET channel after a period of minutes, extending the dynamic range of the channel (15). In bullfrog hair cells, pharmacological up-regulation of cAMP reduced the frequency of spontaneous hair bundle oscillations (16). Furthermore, in humans, a loss of function mutation in adenylyl cyclase 1 (*ADCY1,* an enzyme that catalyzes cAMP production) is associated with hearing loss (17) and zebrafish carrying an equivalent mutation (*adcy1b* morphants) exhibited significantly reduced FM1-43 dye uptake in lateral line hair cells, indicating dysfunctional MET. These studies indicate a potential role for cAMP in modulating MET channel sensitivity in mammals.

In this study, we determine the mechanism of cAMP modulation of the MET channel in a mammalian cochlear hair cell model. We first characterized the cAMP effect in rat outer hair cells (OHCs). Second, we describe a long depolarization manipulation (LDM), which we found mirrored the effects of cAMP up-regulation. Third, by measuring the mechanical changes of the hair bundle, we confirmed that cAMP and long depolarization-induced effects on channel sensitivity are due to a reduction in gating spring stiffness. Finally, we find that cAMP targets the exchange protein directly activated by cAMP (EPAC) rather than protein kinase A (PKA) for modulating MET sensitivity. This cAMP regulation of gating spring stiffness provides a cell signaling means for controlling the sensitivity of MET channels.

Significance

Regulation of auditory sensitivity contributes to the precision, dynamic range, and protection of the auditory system. Regulation of the hair cell mechanotransduction channel is a major contributor to controlling the sensitivity of the auditory transduction process. The gating spring is a critical piece of the mechanotransduction machinery because it opens and closes the mechanotransduction channel, and its stiffness regulates the sensitivity of the mechanotransduction process. In the present work, we characterize the effect of the second-messenger signaling molecule cyclic adenosine monophosphate (cAMP) and identify that it reduces gating spring stiffness likely through an exchange protein directly activated by cAMP (EPAC)-mediated pathway. This is a unique physiologic mechanism to regulate gating spring stiffness.

Author affiliations: [a]Department of Physiology and Biophysics, University of Colorado Anschutz Medical Campus, Aurora, CO 80045; and [b]Neuroscience Graduate Program, University of Colorado Anschutz Medical Campus, Aurora, CO 80045

Author contributions: A.A.M., G.A.C., and A.W.P. designed research; A.A.M., G.A.C., and A.W.P. performed research; A.A.M., G.A.C., and A.W.P. analyzed data; and A.A.M., G.A.C., and A.W.P. wrote the paper.

The authors declare no competing interest.

This article is a PNAS Direct Submission.

[1]A.A.M. and G.A.C. contributed equally to this work.

[2]To whom correspondence may be addressed. Email: anthony.peng@cuanschutz.edu.

This article contains supporting information online at http://www.pnas.org/lookup/suppl/doi:10.1073/pnas.2107567119/-/DCSupplemental.

Published July 19, 2022.

Results

cAMP Regulation of Mammalian MET. To characterize the cAMP effect in rat OHCs, we recorded MET currents and hair bundle displacements in response to a family of fluid-jet (FJ) force steps and generated activation curves before and after bath application (10 min) of hydrolysis-resistant cAMP analogs (0.1 mM 8-Bromoadenosine 3′,5′-cyclic monophosphate, 8-BrcAMP, or dibutyryl cyclic adenosine monophosphate, dbcAMP) (Fig. 1*A* and *B*). In rat OHCs, 8-BrcAMP produced both a rightward shift in the half activation (from 25.1 ± 6.3 nm to 38.6 ± 5.4 nm, $n = 6$, $P = 0.0033$, paired t test) (Fig. 1*C*) and increased width (from 53.6 ± 13.3 nm to 76.2 ± 20.8 nm, $P = 0.0025$, paired t test) (Fig. 1*D*) of the activation curve. To further support a cAMP pathway-specific effect, we repeated these experiments using 0.1 mM dbcAMP. Consistent with the results from 8-BrcAMP, 0.1 mM dbcAMP produced a rightward shift in the half-activation (from 27.3 ± 4.8 nm to 56.6 ± 18.7 nm, $n = 9$, $P = 0.0011$, paired t test) (Fig. 1*C*) and increased width (from 66.5 ± 13.9 nm to 97.6 ± 20.1 nm, $P = 0.0057$, paired t test) (Fig. 1*D*) of the activation curve.

Consistent with a right-shifted activation curve, resting open probability measurements from cells treated with 8-BrcAMP and dbcAMP were significantly decreased (8-BrcAMP: from 5.3 ± 1.1% to 3.7 ± 0.9%, $P = 0.0025$, paired t test; dbcAMP: from 5.1 ± 0.9% to 2.6 ± 1.2%, $P = 0.00025$, paired t test) (Fig. 1*E*). It is important to note that we also observed that in our control condition (Norm Ext), the resting open probability showed a statistically significant decrease (Norm Ext: from 5.0 ± 1.0% to 4.0 ± 0.9%, $n = 8$, $P = 0.043$, paired t test) (Fig. 1*E*). However, one-way ANOVA analysis with Tukey–Kramer post hoc test for multiple comparisons revealed that the change in resting open probability between the two time points was significantly different for control and dbcAMP, but not between control and 8-BrcAMP ($P = 0.014$ for control vs. dbcAMP, $P = 0.42$ for control vs. 8-BrcAMP, $P = 0.28$ for 8-BrcAMP vs. dbcAMP) (*SI Appendix*, Fig. S1*D*), suggesting a true effect of dbcAMP on resting open probability beyond the decrease we observed in the control condition. Furthermore, we performed one-way ANOVA analyses for the other summary data presented in Fig. 1. All one-way ANOVA with post hoc comparisons were consistent with a statistically significant effect of dbcAMP vs. the control (*SI Appendix*, Fig. S1).

Adaptation of the MET process is hypothesized to extend the dynamic range and increase the frequency selectivity of the hair cell (11–13). Experimentally, adaptation manifests as a decay of the MET current in response to a constant stimulus and a rightward shift of the activation curve. We analyzed the amount of MET current decay in response to cAMP analogs before and after applying either 8-BrcAMP or dbcAMP. We observed a nonstatistically significant trend toward increased adaptation with 0.1 mM 8-BrcAMP (from 21.4 ± 8.9% to 29.1 ± 13.2%,

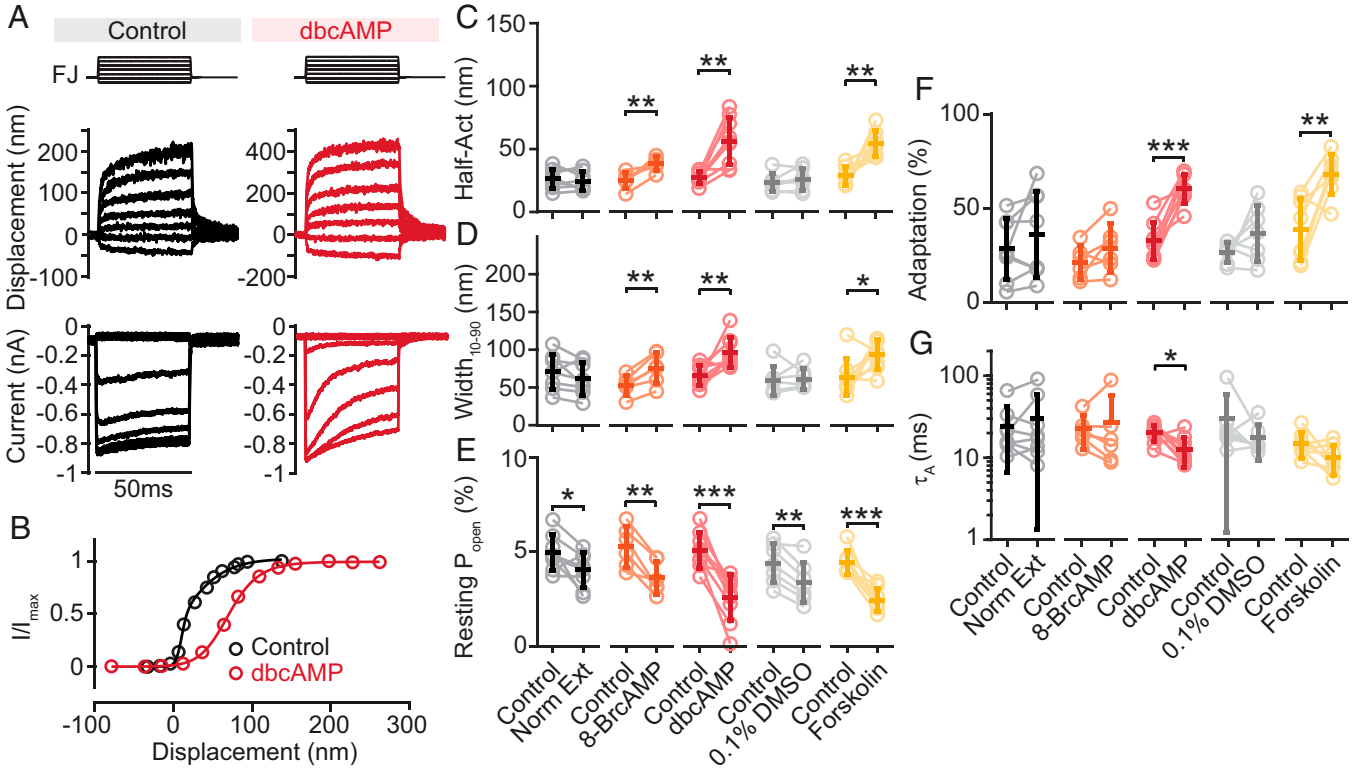

Fig. 1. cAMP regulation of mammalian MET. (*A*) Example traces of hair bundle displacement and MET currents from a rat OHC elicited by FJ force steps. Control traces were obtained 5 min after entering whole-cell mode. Normal external solution (Norm Ext) or different drugs (dbcAMP in this example) were then perfused for 10 min, and a second dataset was collected 15 min after entering whole-cell mode. (*B*) MET current versus hair bundle displacement (activation curve) for the data presented in *A*. (*C* and *D*) Summary plots for the half activation (Half-Act) and 10–90 width ($Width_{10–90}$) of the activation curve obtained from control (Norm Ext), 0.1% DMSO control, and experimental conditions. 8-BrcAMP, dbcAMP, and forskolin were used at 0.1 mM concentrations. Number of cells: control $n = 8$, 0.1% DMSO control $n = 7$, 8-BrcAMP $n = 6$, dbcAMP $n = 9$, forskolin $n = 8$. 8-BrcAMP, dbcAMP, and forskolin produced a rightward shift in the half-activation ($P = 0.0033$, $P = 0.0011$, $P = 0.0025$, paired t tests) and increased the 10–90 width of the activation curve ($P = 0.0025$, $P = 0.0057$, $P = 0.04$, paired t tests), while control and DMSO cells showed no change. (*E*) Resting P_{open} summary data from cells in all conditions. (*F* and *G*) Adaptation magnitude and time constant (τ_A) summary data for a FJ stimulation that produced ~50% of the maximum recorded current for that cell (50% I_{max}). dbcAMP and forskolin, but not 8-BrcAMP, produced a significant increase in adaptation magnitude ($P = 1.2E\text{-}4$, $P = 0.0041$, paired t tests), while control and DMSO cells showed no change. dbcAMP also reduced the adaptation time constant ($P = 0.017$). Error bars indicate the mean ± SD. *$P \leq 0.05$, **$P \leq 0.01$, ***$P \leq 0.001$.

$P = 0.11$, paired t test) (Fig. 1*F*). However, dbcAMP produced a statistically significant increase in adaptation magnitude (from 33.0 ± 9.8% to 60.9 ± 7.8%, $P = 0.00011$, paired t test) (Fig. 1*F*). When using FJ stimulation, we previously determined that a single exponential provided the best fit to the MET current decay, with time constants on the order of tens of milliseconds consistent with slow adaptation (18, 19). In response to 8-BrcAMP application, the adaptation time constant was unchanged (from 22.8 ± 10.1 ms to 26.7 ± 30.4 ms, $P = 0.67$, paired t test) (Fig. 1*G*), but was significantly decreased when dbcAMP was used (from 20.4 ± 4.7 ms to 12.8 ± 5.2 ms, $P = 0.017$, paired t test) (Fig. 1*G*).

The results from experiments with cAMP analogs suggest that cAMP can regulate the MET process. However, these experiments do not provide evidence of a physiologically relevant mechanism, such that cAMP can be endogenously generated within the hair cell to regulate MET. Therefore, we performed similar experiments with 0.1 mM forskolin, a pharmacological stimulator of endogenous adenylyl cyclases that increases the intracellular concentration of cAMP. Adenylyl cyclase isoforms 1, 6, and 9 have been shown to be expressed in the rat organ of Corti, with some evidence of adenylyl cyclase 1 and 6 localizing to the stereocilia of both inner hair cells (IHC) and OHCs (17, 20–22). We found that forskolin produced similar results as the cAMP analogs on the activation curve [Half-Act, from 28.8 ± 7.3 nm to 54.5 ± 10.3 nm, $n = 8$, $P = 0.0025$, paired t test (Fig. 1*C*); width, from 64.3 ± 25.0 nm to 94.5 ± 19.9 nm, $P = 0.040$, paired t test (Fig. 1*D*); resting open probability, from 4.5 ± 0.64% to 2.5 ± 0.62%, $P = 0.00058$, paired t test (Fig. 1*E*)] and slow adaptation (magnitude, from 38.9 ± 16.6% to 68.4 ± 10.8%, $P = 0.0041$, paired t test) (Fig. 1*F*). Although the resting open probability was significantly decreased in the 0.1% DMSO control condition (from 4.4 ± 1.1% to 3.4 ± 1.1%, $n = 7$, $P = 0.0014$, paired t test) (Fig. 1*E*), the magnitude of the change in resting open probability between DMSO and forskolin was significantly different ($P = 0.028$, unpaired, unequal variance t test) (*SI Appendix*, Fig. S1*D*). The adaptation time constant was not significantly different for 0.1% DMSO ($P = 0.29$, paired t test) (Fig. 1*G*) or with 0.1 mM forskolin ($P = 0.09$, paired t test) (Fig. 1*G*). Together, these data indicate that in rat OHCs, the cAMP second messenger is an endogenous mechanism that regulates the sensitivity of the MET channel. Since dbcAMP and forskolin produced the most consistent effects, we predominantly used these compounds in subsequent experiments in this study.

Long Depolarization and cAMP Have Similar Effects on MET. Previously, we reported that depolarizing a hair cell to +76 mV produces a transient increase in MET channel resting open probability that subsequently decays over a period of several seconds (23, 24). In this previous work, we attributed the increase in resting open probability, which has a time course exceeding 100 ms, to a mechanism involving the lipid membrane, but we did not investigate the decay in resting open probability. Here, we describe the effect of the decay in resting open probability at depolarized potentials that occurs during a depolarization of ∼10 s or longer, which we term "long depolarization modulation" or LDM.

We subjected OHCs to LDM, and using a stiff probe, we elicited MET current families to generate activation curves at various time points during the depolarization (*SI Appendix*, Fig. S2). We observed that during the prolonged depolarization, the activation curve shifted rightward and became less sensitive, which remained upon repolarization. To compare the effect before and after LDM, we performed experiments using the FJ that were similar to our experiments with cAMP analogs (Fig. 2*A* and *B*, black and gray traces). The activation curve as measured with the FJ (Fig. 2*B*) exhibited both a significant rightward shift (Fig. 2*C*) (Half-Act, from 32.8 ± 14.7 nm to 59.8 ± 17.7 nm, $P = 2.0E\text{-}5$, paired t test) and increased width after depolarization (Fig. 2*C*) ($Width_{10–90}$, from 70.8 ± 19.7 nm to 95.1 ± 26.2 nm, $P = 0.039$, paired t test). Resting open probability was similarly decreased (Fig. 2*E*) (Resting P_{open}, from 4.7 ± 1.9% to 1.6 ± 1.0%, $P = 1.3E\text{-}5$, paired t test), while peak current was unchanged (Fig. 2*D*) (from 0.75 ± 0.08 nA to 0.73 ± 0.11 nA, $P = 0.37$, paired t test). To determine the effect of LDM on MET adaptation, we first examined the effect on fast adaptation using stiff probe stimuli before and after LDM and found no effect on fast adaptation (*SI Appendix*, Fig. S3).

Next, we investigated the effect of LDM on slow adaptation. Using 50-ms step-like FJ stimuli (Fig. 2*A*), we found that following LDM the adaptation magnitude was significantly increased (Fig. 2*E*) (Adaptation %, from 32.8 ± 21.4% to 70.9 ± 9.0%, $n = 15$, $P = 5.5E\text{-}7$, paired t test) and adaptation time constants were significantly decreased (Fig. 2*E*) (τ_A, from 20.1 ± 9.1 ms to 9.7 ± 2.6 ms, $P = 4.0E\text{-}4$, paired t test). All of the LDM effects mirrored the cAMP up-regulation effects, raising the possibility that these two manipulations activate a similar mechanism.

cAMP and LDM Are Not Additive. We hypothesized that cAMP and depolarization operate through or engage a common mechanism regulating the MET channel in hair cells. Therefore, we predicted that activation of the cAMP pathway prior to LDM would prevent any further change to MET. Indeed, we found that in OHCs exposed to 0.1 mM dbcAMP, activation curve width, resting open probability, slow adaptation magnitude, and slow adaptation time constant were not significantly different after LDM (dbcAMP, $Width_{10–90}$, $P = 0.97$; Resting P_{open}, $P = 0.23$; % Adaptation, $P = 0.58$; τ_A, $P = 0.23$; $n = 12$, paired t tests) (Fig. 2*C–E*). In dbcAMP-treated cells, activation curve half activation was slightly right-shifted after depolarization (Fig. 2*C*) (from 46.7 ± 14.8 nm to 55.7 ± 12.3 nm, $P = 0.038$, paired t test), but the magnitude of the shift was significantly smaller from that in control cells ($P = 0.0044$, unpaired t test). With multiple methods to affect the resting open probability and magnitude of adaptation, we observed a negative linear correlation between the resting open probability and the magnitude of slow adaptation that a cell exhibited ($r = -0.62$, $P = 2.89E\text{-}16$) (Fig. 2*F*). These data suggest that in rat OHCs, the resting open probability can predict the amount of slow adaptation the cell will exhibit when stimulated with 50-ms duration FJ step stimuli. Together, these data demonstrate that cAMP and LDM are not additive, supporting the hypothesis that LDM and cAMP modulate the same mechanism.

cAMP Reduces the Stiffness of the Hair Bundle. The rightward shift and increased width of the activation curve are consistent with a decrease in gating spring stiffness. The total stiffness of the hair bundle (k_{HB}) is dictated by at least two structural components that exert forces with opposite vectors: the stiffness of gating springs (k_{GS}), which exerts a force in the negative direction, pulling the hair bundle in the direction of the shortest row of stereocilia, and the stiffness of stereocilia pivots (k_{SP}), which imposes a resistive force in the opposite direction of the gating spring force. According to gating spring theory (6), a decrease in gating spring stiffness increases the width of the activation curve and would result in a movement of the hair bundle toward the tallest row of stereocilia (Fig. 3*A* and *C*). As the contributions of k_{GS} (Fig. 3*A*) and k_{SP} (Fig. 3*B*) to the total hair bundle stiffness (k_{HB}) decreases or increases, we can identify relative movements of the hair bundle and changes in k_{HB}. Importantly, only changes to the gating

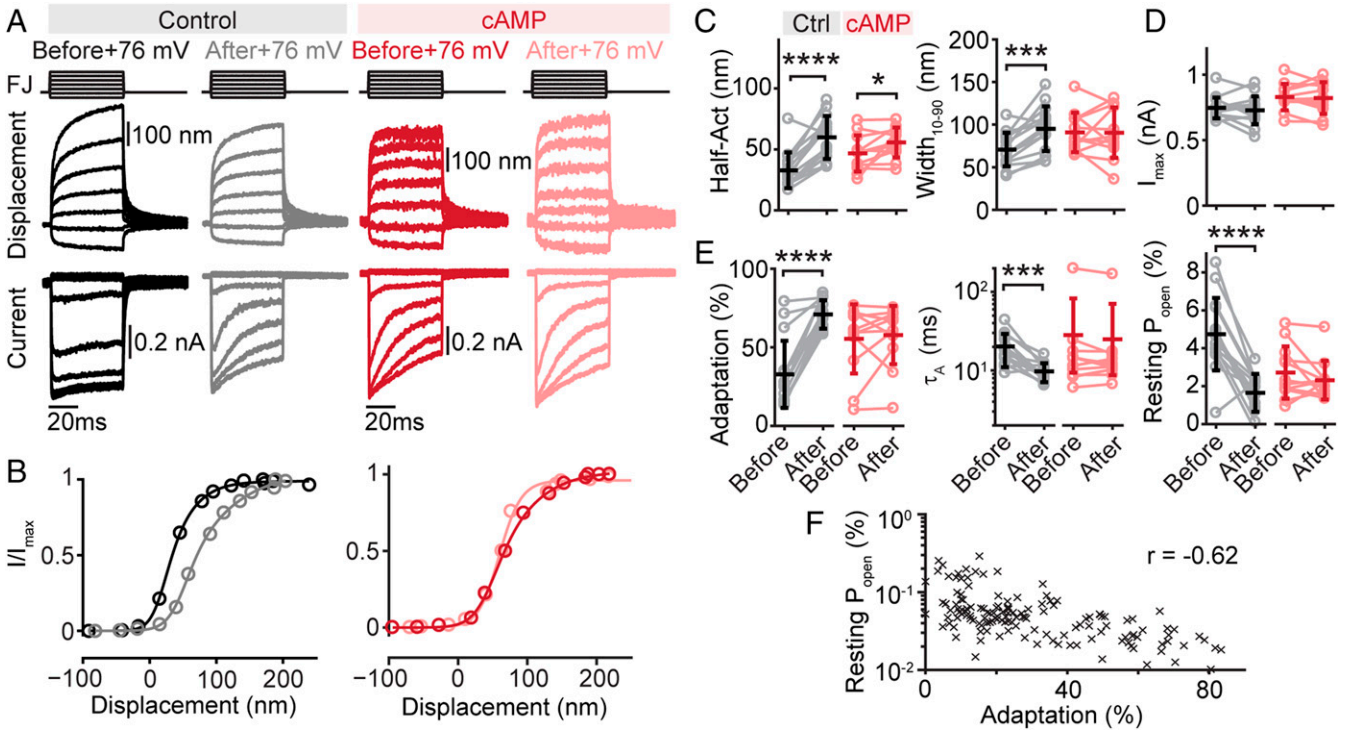

Fig. 2. LDM and cAMP up-regulation are not additive. (*A*) Hair bundle displacement and current traces from a rat OHC elicited by FJ stimulation before and immediately after a long +76 mV depolarization. "FJ" denotes the stimulus waveform. Data in red are cells treated with either 0.1 mM dbcAMP or forskolin. (*B*) Activation curves from data in *A*. (*C*) Activation curves show a rightward shift (Half-Act, P = 2.0E-5, paired t test, n = 15) and increased width ($Width_{10–90}$, P = 1.2E-4, paired t test) after depolarization. Activation curves from cAMP-treated cells show a slight rightward shift (P = 0.04, paired t test, n = 12), but no change in width (P = 0.97, paired t test). (*D*) Peak MET current size was unchanged after depolarization for both control and cAMP-treated cells (I_{max}, control, P = 0.37, cAMP, P = 0.72, paired t tests). (*E*) Depolarization significantly increased the adaptation magnitude (Adaptation %, P = 5.5E-7, paired t test), decreased the slow adaptation time constant (τ_A, P = 4.0E-4, paired t test), and decreased the resting open probability (Resting P_{open}, P = 1.3E-5, paired t test) in control cells, while cAMP-treated cells showed no change (Adaptation %, P = 0.58; τ_A, P = 0.23; Resting P_{open}, P = 0.23, paired t tests). (*F*) In rat OHCs, resting open probability negatively correlates with slow adaptation magnitude (r = −0.62, P = 2.89E-16. Cell numbers: Control, 1 mM BAPTA n = 82, 10 mM BAPTA, n = 16; 0.1 mM BAPTA, n = 8; with 0.1 mM dbcAMP or forskolin, 1 mM BAPTA, n = 19, 10 mM BAPTA, n = 8, 0.1 mM BAPTA, n = 8). Error bars indicate the mean ± SD. *$P \leq 0.05$, ***$P \leq 0.001$, ****$P \leq 0.0001$.

spring stiffness would result in changes in the activation curve since changes to k_{SP} do not modify gating (Fig. 3*C*) (5, 6, 25).

To further support the hypothesis that the gating spring stiffness is decreased with cAMP up-regulation and LDM, we measured the relative change in total hair bundle stiffness with FJ hair bundle stimulation and high-speed imaging at 5 min after entering whole-cell mode (control) followed by 10 min of 0.2 mM dbcAMP application (dbcAMP) (Fig. 3*D*). In these experiments, extreme care was used to ensure that the position of the FJ in relation to the hair bundle (in *X*, *Y*, and *Z*) was consistent between the 5-min and 10-min postdrug conditions so that the force from the FJ on the hair bundle remained consistent between the two time points. This allowed us to use the driving voltage command to the FJ piezo as a proxy for the relative force on the hair bundle. These values only apply to a given cell and cannot be compared across different cells due to the different hair bundle morphologies and characteristics and positioning of the FJ in each given hair cell; therefore, we normalized the stiffness values against the control condition for each cell. We plotted driver voltage against the hair bundle displacement at the end of the 50-ms FJ step, where the displacement is more stable, and fit this with a linear equation (forced through the origin). The relative stiffness of the hair bundle was unchanged when no drug was present (Fig. 3*E* and *G*) (11 ± 30%, n = 7) but significantly decreased when 0.2 mM dbcAMP was perfused (Fig. 3*F* and *H*) (−13 ± 12%, n = 11). To gain some insight into the size of the change, we estimated the total hair bundle stiffness in the control conditions by calibrating the FJ force (26). We found a hair bundle stiffness of 6.3 ± 1.3 mN/m (n = 6), similar to previous results (26, 27). With the observed 13% decrease in stiffness with cAMP up-regulation, the hair bundle stiffness would decrease to 5.5 mN/m.

We also assayed the effect of LDM on total hair bundle stiffness using the same method as in Fig. 3*D*–*H*. We found that LDM significantly decreased the total stiffness of the hair bundle in control cells (−22 ± 15%, n = 15) but had no effect in dbcAMP-treated cells (2 ± 19%, n = 12) (Fig. 3*I*), which further supports that the two manipulations are not additive. With these changes in total hair bundle stiffness, it was surprising not to see any consistent effects on the kinetics of the hair bundle movement (*SI Appendix*, Fig. S4). It could be that the changes in hair bundle mechanics were not large enough to elicit a sufficient change in the movement kinetics. In summary, these data demonstrate that after cAMP up-regulation or LDM, hair bundle stiffness decreased, consistent with a decrease in k_{GS} or k_{SP}.

To delineate between an effect on k_{GS} or k_{SP}, we tested whether the changes in hair bundle stiffness were correlated with changes in the activation curve. The inverse of the width of the activation curve is linearly related to k_{GS} (*SI Appendix*, *Materials and Methods*). We indeed found that k_{GS} and 1/width are correlated (Fig. 3*J*) (r = 0.57, P = 4.6E-5). These data suggest that gating spring stiffness is decreased upon cAMP up-regulation or LDM.

LDM Results in Decreased Gating Spring Stiffness. The shorter timescale of the LDM process allows continuous monitoring of

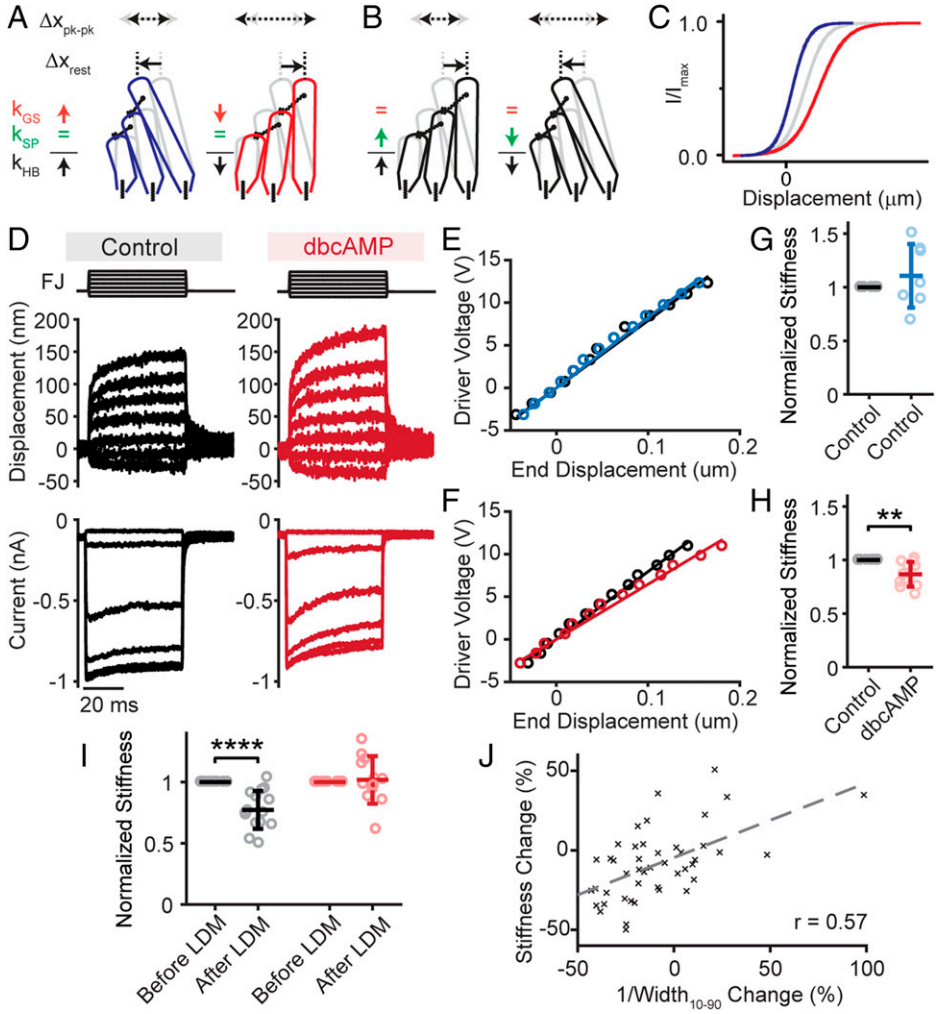

Fig. 3. Pharmacological up-regulation of cAMP reduces the stiffness of the hair bundle. (*A* and *B*) Graphical summary of the possible experimental outcomes of modifying the relative contributions [increase (↑), decrease (↓), or remain the same (=)] of the gating springs (k_{GS}; *A*) or the stereocilia pivots (k_{sp}; *B*) to the total hair bundle stiffness (k_{HB}). In each schematic, the gray hair bundle is the control, and the dark hair bundle outline illustrates the change in the hair bundle due to the manipulation with illustrations of the resting position movement (Δx_{rest}) and change in the peak-to-peak displacement of the hair bundle given the same force stimulus ($\Delta x_{pk\text{-}pk}$). (*C*) Theoretical changes in the activation curve for when gating spring increases (blue) and decreases (red) from the control condition (gray). No changes in the activation curve are expected for k_{SP} changes. (*D*) Example hair bundle displacement and MET current traces from a rat OHC before and after 10 min of 0.2 mM dbcAMP perfusion. (*E*) Hair bundle stiffness measurement (FJ driver voltage/hair bundle ending displacement) for a control cell at 5 (black) and 15 (blue) min. (*F*) Hair bundle stiffness measurement for the 0.2 mM dbcAMP-treated cell shown in *D*. Notice the decreased slope after dbcAMP treatment. (*G*) Summary plots showing no change in hair bundle stiffness for control cells at 5 and 15 min (n = 7, P = 0.38, paired t test) and (*H*) a decrease in hair bundle stiffness for cells treated with 0.2 mM dbcAMP after 10 min (n = 11, P = 0.0034, paired t test). (*I*) Depolarization decreases hair bundle stiffness in control cells (P = 0.000056, paired t test), but not in cAMP-treated cells (P = 0.76, paired t test). (*J*) Plot showing the correlation (r = 0.57, P = 4.6E-5) between the stiffness change in the hair bundle and the $1/Width_{10\text{–}90}$, which is proportional to Z in a single Boltzmann fit and is linearly correlated to k_{GS} according to the gating spring theory. All cells from *G–I* are included. Dashed line is the best linear fit (slope = 0.47, y-int = −4.56). Error bars indicate the mean ± SD. **$P \leq 0.01$, ****$P \leq 0.0001$.

the mechanical changes of the hair bundle over a period of seconds. Delivering cAMP drugs by a perfusion system over the course of minutes precludes accurate resting position measurements because the movement noise is too high on that timescale. With the shorter activation time of LDM over the time course of ∼10 s, we designed an experiment to monitor the changes in the stiffness of the hair bundle, the resting position of the hair bundle, and the change in the activation curve simultaneously (Fig. 4*A*). Using our high-speed imaging technique and FJ stimulation (19), we subjected rat OHCs to intermittent sine wave stimuli of the same fluid drag force during LDM. Upon depolarization to +76 mV, the resting open probability increased to a maximum of 51.4 ± 8.9% (Fig. 4*D*, black trace, and Fig. 4*F*) ("1st +76 mV" summary data n = 36), after which it decreased to a steady state of 23.3 ± 12.1% (Fig. 4*G*) ($\Delta P_{open}^{+76\ mV}$, −28.1 ± 10.4%). This decrease in resting open probability indicates the rightward shift of the activation curve. Concurrently, the hair bundle underwent mechanical changes that developed over a time course similar to the decline in resting open probability during the depolarization (Fig. 4*E*). In response to sine wave stimulations of identical driver voltage, the resting position of the hair bundle moved forward (Fig. 4*D*, *E*, and *H*) ($\Delta x_{rest}^{-84\ mV}$, 27.3 ± 30.4 nm), and the normalized displacement of the hair bundle increased (Fig. 4*D*, *E*, and *I*) ($x_{pk\text{-}pk}^{end}/x_{pk\text{-}pk}^{start}$, 1.20 ± 0.16), indicating that total hair bundle stiffness decreased, which is consistent with our previous observations (Fig. 3*H*). We observed a small increase in hair bundle stiffness immediately upon depolarization (first +76 mV, 3.6 ± 7.2%), which differed from a previous report (27). Similar observations on resting position and total hair bundle stiffness were made when 10 mM intracellular BAPTA was used (*SI Appendix*, Fig. S5*A–D*). The observation that the resting position increases with a decrease in total hair bundle stiffness is only consistent with the hypothesis that LDM decreases k_{GS} (Fig. 3*A* and *B*).

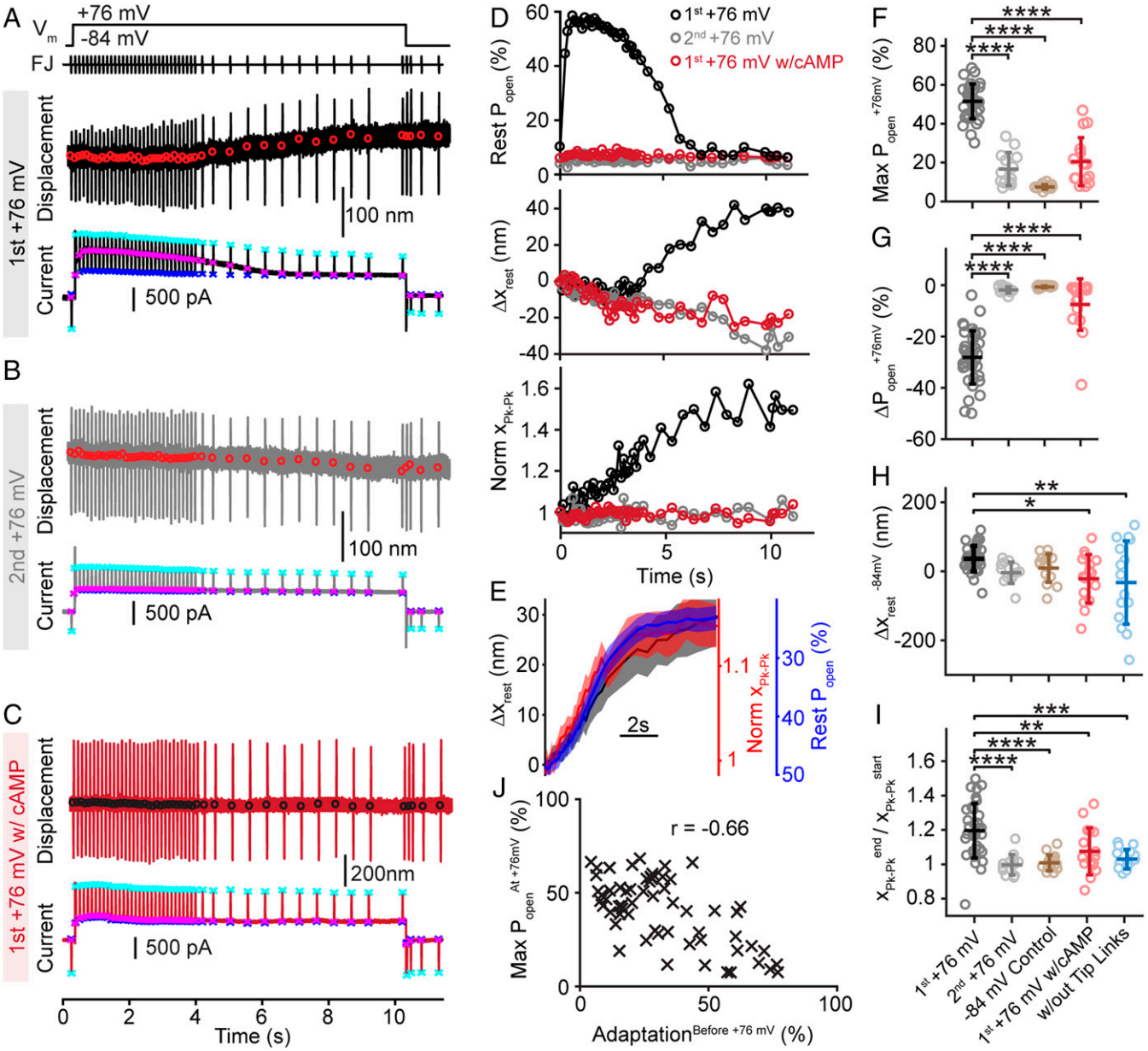

Fig. 4. LDM reduces the stiffness of the gating springs. (*A–C*) Traces for measured displacement and current during a long depolarization to +76 mV that is stimulated intermittently with a single sine wave cycle of constant force magnitude. Circles in the displacement trace track the resting position of the hair bundle before each sine wave stimulus. Xs in the current trace indicate the resting current (magenta), negative displacement current (blue), and positive displacement current (cyan). Cell's response to the first presentation of the +76-mV protocol (*A*), response to the second +76-mV presentation (*B*), and a dbcAMP-treated cell's response to the first +76-mV presentation (*C*). (*D*) Quantification of the change in resting open probability (Rest P_{open}), hair bundle resting position (Δx_{rest}), and normalized displacement size (Norm $x_{pk\text{-}pk}$) from the traces presented in *A–C*. (*E*) Average and SE (shade) for the three parameters in *D* for the first +76-mV protocol ($n = 36$) show a similar time course of changes from 1 to 10 s. Note that the resting open probably axis was inverted. (*F–I*) Summary plots for the maximum P_{open} (one-way ANOVA, $P = 1.6E\text{-}28$), the change in resting P_{open} at +76 mV (max P_{open} minus the average resting P_{open} before repolarization, $P = 7.2E\text{-}20$), the change in hair bundle resting position (Δx_{rest}, $P = 0.0030$), and the normalized hair bundle displacement at the end of the protocol ($x_{pk\text{-}pk}^{end}/x_{pk\text{-}pk}^{start}$, $P = 8.5E\text{-}8$) for rat OHCs. In summary plots, "1st +76 mV" and "2nd +76 mV" refer to either the first ($n = 36$) and second presentation ($n = 13$) of the +76-mV protocol, respectively, in the same cell. "−84 mV Control" ($n = 15$) are cells that received the same FJ stimulation protocol but were not depolarized. "1st +76 mV w/cAMP" ($n = 16$) are cells treated with either 0.1 mM dbcAMP or forskolin before the +76-mV protocol. "w/out Tip-Links" ($n = 15$) are cells that were subjected to calcium chelator before the +76-mV protocol. Significance bars are based on Tukey–Kramer post hoc test. (*J*) Correlation plot demonstrating a linear relationship between the amount of slow adaptation before depolarization and the maximum P_{open} achieved at +76 mV ($r = -0.66$, $P = 5.62E\text{-}9$; cell numbers: Control, 1 mM BAPTA, $n = 25$; 10 mM BAPTA, $n = 6$; 0.1 mM dbcAMP or forskolin, 1 mM BAPTA, $n = 16$; 10 mM BAPTA, $n = 4$; 0.1 mM BAPTA, $n = 5$). Error bars indicate the mean ± SD. $^*P \le 0.05$, $^{**}P \le 0.01$, $^{***}P \le 0.001$, $^{****}P \le 0.0001$.

To increase our confidence in these data, we performed several control experiments to ensure that the mechanical changes observed were not an artifact. First, we performed the same mechanical protocol but did not depolarize the cell (Fig. 4*F–I*, brown circles) ("−84 mV Control"). Next, the effects of depolarization on resting open probability and hair bundle mechanics only occur for hair cells that have not been recently depolarized, since after inducing LDM, the cell requires time (on the order of minutes) to return from the effects of LDM with the rate depending on the intracellular BAPTA concentration (*SI Appendix*, Fig. S5*E–G*). Therefore, subsequent depolarizations delivered immediately following the initial depolarization have little to no effect (Fig. 4*A*, *B*, and *D*, gray) ("2nd +76 mV"). Third, cells that were treated with either 0.1 mM dbcAMP or forskolin did not exhibit the increase in resting open probability, change in resting open probability during the depolarization, or changes in hair bundle mechanics (Fig. 4*D*, red)

("1st Presentation w/cAMP"), and appeared like a cell that was already subjected to LDM (Fig. 4*B*, *F*–*I*, comparing gray and red) (Max $P_{open}^{+76\ mV}$, $P = 0.65$; $\Delta P_{open}^{+76\ mV}$, $P = 0.27$; $\Delta x_{rest}^{-84\ mV}$, $P = 0.95$; $x_{pk\text{-}pk}^{end}/x_{pk\text{-}pk}^{start}$, $P = 0.40$, Tukey–Kramer post hoc test). This observation also supports that the activation of the cAMP pathway and LDM function through the same mechanism.

Finally, we repeated these experiments after calcium-chelator treatment (EDTA) via iontophoresis to sever tip links and, therefore, the gating springs (18, 26, 28). Hair bundles that lack tip links only have k_{SP} contributing to the hair bundle stiffness and should not exhibit any of the mechanical changes in response to LDM that modulates gating springs. EDTA-treated hair bundles exhibited neither the positive change in resting position nor the increase in displacement size after depolarization (Fig. 4*H*–*I*, comparing black to blue) ($\Delta x_{rest}^{-84\ mV}$, $P = 0.0055$; $x_{pk\text{-}pk}^{end}/x_{pk\text{-}pk}^{start}$, $P = 0.00017$, Tukey–Kramer post hoc test). This experiment also indicates that in the absence of tip links, LDM does not change hair bundle stiffness, suggesting that LDM does not affect k_{SP}. One-way ANOVA analysis revealed statistical significance for all measured parameters (Fig. 4*F*–*I*), indicating that the experimental condition of LDM was different from the control conditions. Together, these control experiments provide evidence that the mechanical changes we observed are real, thus indicating that LDM causes a decrease in gating spring stiffness.

In all experiments performed in Fig. 4, we observed a negative correlation between the maximum resting open probability that a cell exhibited during the depolarization (typically occurring in the first second (Fig. 4*D*, black) and the amount of adaptation that the cell exhibited before being depolarized. In other words, OHCs that exhibited smaller magnitudes of slow adaptation before being depolarized typically displayed higher maximum resting open probability values upon depolarization (Fig. 4*J*) ($r = -0.66$, $P = 5.62\text{E-}9$). Higher maximum resting open probability suggested that the cell was further from the LDM state, consistent with a lower adaptation magnitude. This finding supports that cells may exist in a continuum of states where LDM moves the cell toward exhibiting a larger slow adaptation magnitude and lower maximum resting open probability.

cAMP and LDM Decrease the Contribution of the Gating Springs to Total Hair Bundle Stiffness. A third method to confirm a change in k_{GS} was to measure the contribution of k_{GS} to k_{HB} by disrupting tip links. We performed experiments where hair cells were either depolarized or treated with 0.2 mM dbcAMP, and we measured hair bundle displacements before and after severing tip links with iontophoresis of the calcium-chelator EDTA (26, 28). Assuming the stiffness of the hair bundle after EDTA treatment is only comprised of k_{SP}, we can then calculate the contribution of k_{GS} to k_{HB} (see *SI Appendix, Materials and Methods* for calculation). If LDM and cAMP decrease k_{GS}, then we would expect k_{GS}/k_{HB} to decrease after LDM or cAMP up-regulation. Hair bundle displacements were measured in response to nonsaturating sinusoidal FJ stimulation before and after a 7-s iontophoretic application of EDTA (Fig. 5*B*, *D*, and *G*). In all experiments, patch-clamp recording of the MET current was used to ensure near-complete tip-link breakage, as measured by MET currents in response to saturating FJ stimuli after the iontophoresis protocol (Fig. 5*B*, *C*, and *F*). Cells with >75 pA of MET current remaining after EDTA treatment were not included for analysis. Consistent with our hypothesis, we found that LDM or dbcAMP treatment caused a decreased k_{GS}/k_{HB} compared with controls (Fig. 5*E*) (IHCs, control, 0.58 ± 0.067, depolarized, 0.49 ± 0.10, $P = 0.042$) (Fig. 5*F*) (OHCs, control, 0.56 ± 0.06, dbcAMP, 0.42 ± 0.13, $P = 0.011$, unpaired, unequal variance *t* tests). Together, both depolarization in IHCs, and dbcAMP treatment in OHCs, reduced the contribution of the gating springs to the total stiffness of the hair bundle, indicating that both manipulations decreased the stiffness of the gating springs.

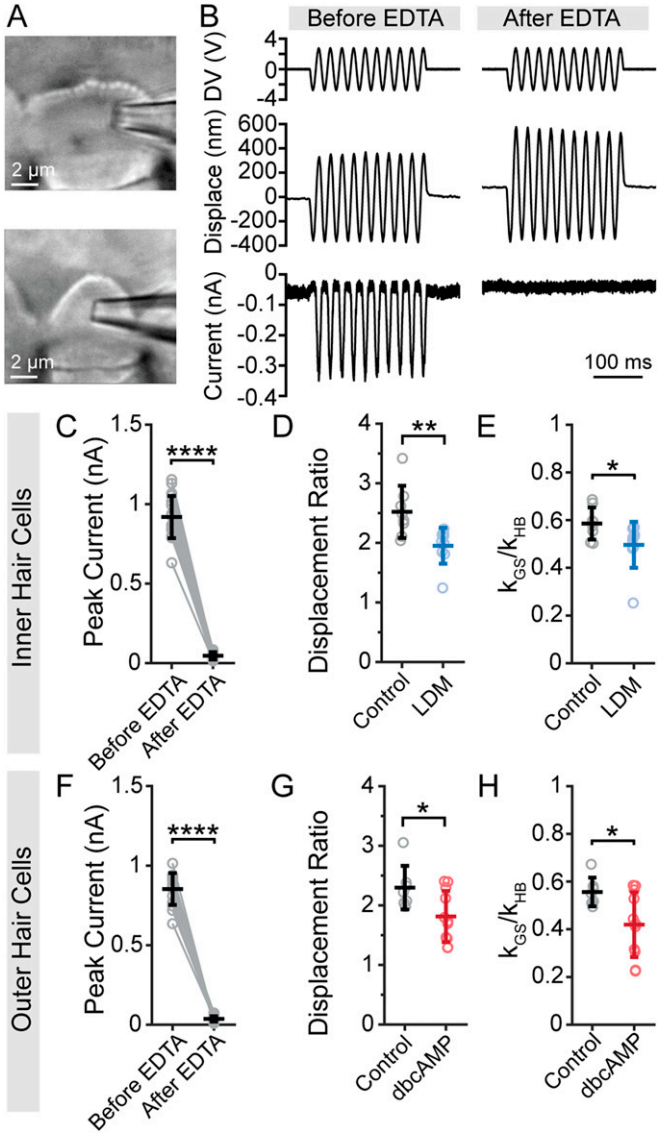

Fig. 5. Depolarization or cAMP reduce the contribution of k_{GS} to k_{HB}. (*A*) Image of the hair bundle with an iontophoretic pipette for an IHC (*Upper*) and OHC (*Lower*). MET currents were recorded in all experiments to measure tip-link disruption. (*B*) Hair bundle displacement and MET current data from the IHC shown in *A* before and after iontophoretic application of EDTA. Notice the change in displacement size and absence of MET current after EDTA. (*C*) EDTA application produced near-complete tip-link breakage (< 75 pA remaining) as measured by the peak MET current in response to a family of force steps (not shown) before and after EDTA treatment ($n = 18$, $P = 4.7\text{E-}16$, paired *t* test). (*D*) IHC bundle displacement size in response to FJ sine wave stimulation increased more after EDTA application in control than after LDM (displacement ratio, control: 2.52 ± 0.44, $n = 8$, LDM: 1.92 ± 0.30, $n = 9$, $P = 0.0093$, unpaired, unequal variance *t* test). (*E*) LDM decreased the contribution of k_{GS} to k_{HB} in IHCs (k_{GS}/k_{HB} from 0.59 ± 0.07 to 0.50 ± 0.1, $P = 0.042$, unpaired, unequal variance *t* test). (*F*) Peak MET current decreased after EDTA treatment in OHCs (0.85 ± 0.1 nA to 0.04 ± 0.02 nA, $n = 15$, $P = 6.4\text{E-}14$, paired *t* test). (*G*) Hair bundle displacement size increased more after EDTA application for control than 0.2 mM dbcAMP-treated OHCs (displacement ratio, control: 2.30 ± 0.37, $n = 7$, dbcAMP: 1.81 ± 0.41, $n = 11$, $P = 0.022$, unpaired, unequal variance *t* test). (*H*) Similar to depolarization, dbcAMP decreases k_{GS}/k_{HB} in OHCs (from 0.56 ± 0.06 to 0.42 ± 0.13, $P = 0.011$, unpaired, unequal variance *t* test). Error bars indicate the mean ± SD. *$P \le 0.05$, **$P \le 0.01$, ****$P \le 0.0001$.

cAMP Modulates MET through EPAC, Not PKA. The classic downstream target of cAMP is PKA, also known as the cAMP-dependent protein kinase. cAMP promotes the dissociation of the regulatory and catalytic subunits of PKA to allow phosphorylation of proteins via the catalytic subunit (29). To determine if the effects we observed with cAMP pharmacology were a result of downstream activation of PKA, we inhibited PKA activity while simultaneously activating the cAMP pathway. Using two different PKA inhibitors, H89 and PKI, we tested if PKA inhibition could prevent the changes in the activation curve observed with cAMP activation. H89 inhibits PKA by competing for the ATP binding site on the catalytic subunit (29). We used H89 at 10 μM, over 200 times its K_i (30) and 10 times greater than the concentration used in IHCs to inhibit PKA modulation of potassium currents (31). At this concentration, data were similar to that using an activator alone (Fig. 6*C–G*, blue) (Half-Act: from 29.1 ± 9.7 nm to 55.0 ± 34.4 nm, $P = 0.013$; $Width_{10–90}$: from 65.1 ± 15.0 nm to 96.8 ± 50.0 nm, $P = 0.038$; Resting P_{open}: from 4.9 ± 0.8% to 3.3 ± 1.4%, $P = 0.0018$; Adaptation: from 22.6 ± 7.8% to 44.7 ± 23.5%, $P = 0.0021$; τ_A: from 28.9 ± 47.5 ms to 12.9 ± 5.9 ms, $P = 0.23$; paired *t* test). PKI is also an inhibitor of the catalytic subunit of PKA by binding to the substrate-binding pocket while unable to be phosphorylated (29). PKI has a K_i of 1.7 nM according to the manufacturer, and we used PKI intracellularly at 1 μM and 5 μM and did not observe any difference. Data with PKI corroborated the data with H89 and were also similar to data with activator alone (Fig. 6*C–G*, purple) (Half-Act: from 29.1 ± 9.0 nm to 60.1 ± 19.8 nm, $P = 0.0013$; $Width_{10–90}$: from 73.7 ± 10.1 nm to 90.6 ± 22.7 nm, $P = 0.048$; Resting P_{open}: from 5.0 ± 1.1% to 3.0 ± 1.3%, $P = 0.0076$; Adaptation: from 24.6 ± 16.7% to 54.1 ± 28.6%, $P = 0.0080$; τ_A: from 31.6 ± 50.6 ms to 15.8 ± 12.6 ms, $P = 0.41$; paired *t* test). Unexpectedly, these data indicate that PKA is not responsible for the rightward shift and increased width of the activation curve observed with cAMP activation.

Another potential cAMP signaling pathway is through the EPAC (32, 33). To test whether EPAC activation can recapitulate the cAMP effect, we used the EPAC-specific agonist 8-(4-Chlorophenylthio)-2′-O-methyladenosine-3′,5′-cyclic monophosphate (8-CPT). 8-CPT is a potent and selective superagonist of EPAC over PKA (34). 8-CPT can be used up to about 10 μM, where there is about 20% activation of PKA and near 100% activation of EPAC (34). When 8-CPT was included in the intracellular solution at 1 μM and 5 μM, hair cells behaved similarly to when the cAMP pathway is activated with dbcAMP or forskolin with a rightward shift of the activation curve and increase in adaptation magnitude over time (Fig. 6, green) (Half-Act: from 38.9 ± 1.9 nm to 56.8 ± 23.8 nm, $P = 0.0087$; $Width_{10–90}$: from 87.8 ± 34.1 nm to 102.1 ± 33.2 nm, $P = 0.046$; Resting P_{open}: from 4.7 ± 1.1% to 3.4 ± 1.5%, $P = 0.013$; Adaptation: from 25.8 ± 10.2% to 48.7 ± 23.9%, $P = 0.0035$; τ_A: from 22.6 ± 15.3 ms to 20.2 ± 12.1 ms, $P = 0.71$; paired *t* test). The results from all three pharmacological manipulations (H89, PKI, and 8-CPT) are consistent with the cAMP effect being mediated by EPAC. We also tested whether there was a baseline level of cAMP activity by using the cAMP inhibitor Rp-cAMPS at 0.1 mM, near the IC_{50} for EPAC1 (35). We found that there was no effect with Rp-cAMPS on the hair cell activation curve (*SI Appendix*, Fig. S6). Taken together, these data suggest that cAMP functions through an EPAC mediated pathway, not PKA, to decrease gating spring stiffness.

Discussion

Regulation of hair cell MET is critical to our auditory system's high precision and wide dynamic range (11–13). Growing evidence indicates the existence of other mechanisms that modulate the activity of the MET channel apart from the classic adaptation processes (24, 36). The present study expands on early work from turtle and bullfrog hair cells (15, 16) and demonstrates that up-regulation of the second messenger cAMP, as well as LDM, modulates the MET channel by decreasing the gating spring stiffness. Data are also consistent with the cAMP effect occurring through activation of EPAC and not the classic PKA mediated pathways.

In this study, we first demonstrated that in rat OHCs, pharmacological agents that increased intracellular cAMP signaling reduced the sensitivity of the MET channel (Fig. 1). We subsequently characterized another manipulation, LDM. Previously, we characterized the changes that occur during depolarization, where there is initially an increase in the resting open probability followed by a subsequent decrease in open probability (24). The increase in resting open probability involved the lipid bilayer and is a separate mechanism from the LDM described here. LDM results in a decline in resting open probability and alters MET properties similarly to cAMP up-regulation (*SI Appendix*, Figs. S2 and S3). We also hypothesize that hair cells exist in a continuum of states where the MET channel resting open probability and the magnitude of slow adaptation are inversely related. Further experiments demonstrated that cAMP up-regulation combined with LDM did not affect MET or hair bundle mechanics in an additive manner, suggesting that the two manipulations act at a common end effector site (i.e., gating spring) to modulate MET (Fig. 2), potentially through different signaling cascades. Both manipulations resulted in decreased MET channel sensitivity, consistent with a decrease in gating spring stiffness (6).

To test the hypothesis of reduced gating spring stiffness, we performed experiments that allowed us to quantify mechanical changes in the hair bundle. In a simplistic view, the stiffness of the hair bundle consists of the contributions of the stiffnesses of the gating springs (k_{GS}) and stereocilia pivots (k_{SP}), which encompasses contributions by other intersterocociliary links as well. The gating springs can contribute ∼50% of the total hair bundle stiffness (18, 26). At rest, the hair bundle position is determined by the tension in the tip link pulling the hair bundle in the negative direction and the resistive force of the stereocilia pivots. Alterations in k_{GS}, but not k_{SP}, are associated with changes in the activation curve (Fig. 3*A–C*). We first found that cAMP up-regulation and LDM were associated with a decrease in hair bundle stiffness, which was correlated with a widening of the activation curve (Fig. 3*J*), all being consistent with an effect on k_{GS}. Next, we found that in response to LDM, the hair bundle exhibited a positive change in the resting position (toward the tallest row of stereocilia) and an increase in the displacement size (Fig. 4), which is consistent with a gating spring stiffness decrease, not a decrease in stereocilia pivot stiffness (Fig. 3*A* and *B*). Additionally, LDM in the absence of tip links did not change the stiffness of the hair bundle, indicating no effect on k_{SP}.

Finally, using an iontophoresis technique to sever tip links, we could estimate the change in the stiffness of the gating springs in response to either cAMP analogs or depolarization by measuring the displacement of the hair bundle in response to a FJ stimulus of the same fluid drag force before and after severing the tip-links. We found that both cAMP and depolarization decreased the contribution of the gating springs to the total hair bundle stiffness (Fig. 5). The gating spring theory posits that changes in gating spring stiffness will result in a change in the MET channel sensitivity (6). With cAMP up-regulation using dbcAMP, we observed a 47% average increase in the width of

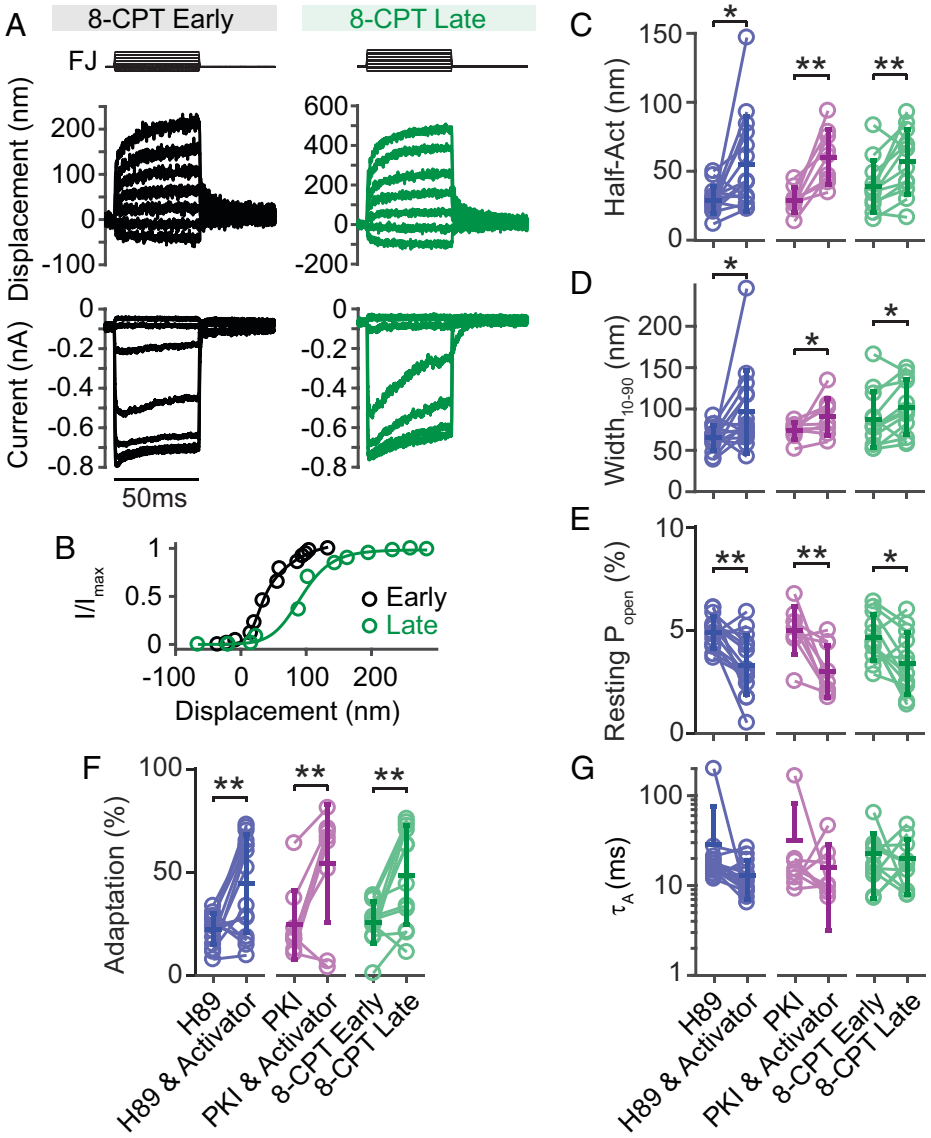

Fig. 6. cAMP modulates MET through EPAC, not PKA. (*A*) Example traces of hair bundle displacement and MET currents from a rat OHC elicited by FJ force steps with 5 μM 8-CPT in the intracellular solution. Early traces were obtained ~5 min after entering whole-cell mode. The late data were collected ~15 min after entering whole-cell mode. (*B*) MET current versus hair bundle displacement (activation curve) for the data presented in *A*. (*C* and *D*) Summary plots for the half activation (Half-Act) and 10–90 width ($Width_{10–90}$) of the activation curve. H89 was used at 0.01 mM, and PKI was used at 1 and 5 μM with either forskolin or dbcAMP as the activator. Data were taken in the presence of the inhibitor and after 10 min of activator application. 8-CPT was used in the intracellular solution at 1 and 5 μM and traces were taken early and late after entering whole-cell mode. Number of cells: H89 and activator $n = 15$, PKI and activator $n = 9$, 8-CPT $n = 12$. H89 and activator, PKI and activator, and 8-CPT produced a rightward shift in the half-activation ($P = 0.013$, $P = 0.0014$, $P = 0.0087$, paired *t* tests) and increased the 10–90 width of the activation curve ($P = 0.038$, $P = 0.048$, $P = 0.046$, paired *t* tests). (*E*) Resting P_{open} summary data from cells in all conditions. (*F* and *G*) Adaptation magnitude and time constant (τ_A) summary data for a FJ stimulation that produced ~50% of the maximum recorded current for that cell (50% I_{max}). H89 and activator, PKI and activator, and 8-CPT produced a significant increase in adaptation magnitude ($P = 0.0021$, $P = 0.0080$, $P = 0.0035$, paired *t* tests). Error bars indicate the mean ± SD. *$P \leq 0.05$, **$P \leq 0.01$.

the activation curve (Fig. 1*D*). According to the gating spring theory, this would be the result of a 32% decrease in gating spring stiffness. When combining the measured changes in k_{HB} (Fig. 3*H*) and k_{GS}/k_{HB} (Fig. 5*I*), we estimate a 34% decrease in k_{GS} on average upon cAMP pathway activation. These two values, which are calculated based on different experimental measures, are consistent with each other, suggesting that k_{GS} changes can account for most of the stiffness changes we observed. These data indicate that cAMP and LDM modulate hair cell MET by decreasing gating spring stiffness.

Knowing that the gating spring is the target of cAMP activation, we sought to determine the signaling pathway. PKA is the classic cAMP target; however, two specific PKA inhibitors were unable to block the cAMP effect (Fig. 6*C*–*G*, blue and purple). Instead, we found that cAMP functions through EPAC to mediate the decrease in gating spring stiffness by using an EPAC-specific activator (Fig. 6, green). Failure of PKA-specific inhibitors to block the cAMP effect along with the specific EPAC activator (8-CPT) mimicking the cAMP effect strongly suggests the EPAC pathway mediating the decreased gating spring stiffness. Ideally, inhibition of the EPAC pathway would help to further support the pathway, however, current inhibitors of the EPAC pathway, like ESI-09 and HJC0197, have general protein denaturing capabilities and may not be competitive inhibitors of EPAC (37). Further experiments are still required to identify an appropriate inhibitor of the pathway, but current data are supportive of an EPAC pathway regulating hair cell MET.

Implications for Auditory Function. cAMP signaling is a ubiquitous pathway in many cell types and serves a variety of different cellular functions. Although the effect of cAMP on MET was documented over two decades ago, the mechanism of action and signaling pathway has not been elucidated until now. These findings provide a potential mechanism for G protein-coupled receptors (GPCRs) to modulate gating spring stiffness and the sound transduction process.

A potential function of the cAMP pathway in hair cells is to provide some level of protection during levels of high-intensity stimulation. cAMP could be up-regulated to decrease MET sensitivity to protect against damage. Another potential pathway could operate through GPCRs and downstream activation of $G_s\alpha$ to stimulate adenylyl cyclase activity to modulate MET activity, but the participation of GPCRs in hair cell MET regulation is yet to be explored.

A resting level of cAMP could allow for bidirectional control of gating spring stiffness, hence hair cell sensitivity. This has been demonstrated to modulate spontaneous oscillation frequency in bullfrog saccular hair cells (16). However, in mammalian hair cells, there does not appear to be a resting level of cAMP activity since Rp-cAMPS, which inhibits both PKA and EPAC (to a lesser extent) activation (35, 38), did not cause a leftward shift in the activation curve (*SI Appendix*, Fig. S6). This result argues against cAMP levels being the determinant of where a given hair cell sits on the continuum of states shown by the resting open probability and baseline level of slow adaptation (Figs. 2*F* and 4*J*); however, this hypothesis cannot be fully ruled out since further experiments using higher concentrations of Rp-cAMPS and different EPAC inhibitors are required.

Potential Molecular Mechanisms of Modulating Gating Spring Stiffness. The molecular and structural composition of the gating springs is still debated (36). The tip link was originally thought to be the gating spring (6), however, electron microscopy and molecular dynamics simulations later suggest that the tip link itself may not be the gating spring due to its rigidity (39, 40). Even more recent data have revived the suggestion that the tip link could contribute to the gating spring (41, 42). Even if the tip link contributes to the gating spring stiffness through the structure of its extracellular domains, it is unlikely to be the target of the cAMP effect since the EPAC signaling pathway is likely restricted to intracellular targets. In addition to the tip link, gating spring stiffness may arise from any component in series with the tip link. Potential elements could be the myosin motors (like myosin VIIa) or their adapter proteins at the upper tip-link insertion point (9, 43, 44), as well as other components at the lower tip-link insertion important for MET, such as CIB2, TMIE, LHFPL5, or TMC1 (2, 3, 45–48). The gating spring stiffness may also potentially arise from its interaction with the lipid bilayer of the stereocilia membrane, where the upper and lower ends of the tip link insert before being anchored to the f-actin core (49). Any of these components could be the target of the EPAC-mediated regulation.

EPAC acts as a guanine exchange factor for the Rap1 and Rap2 small GTPases. Rap has many potential downstream effector pathways, which could lead to modulating gating spring stiffness (33). A notable pathway is one that down-regulates the RhoA signaling pathway to increase smooth muscle relaxation (50) and could target the actin cytoskeleton in hair bundles. More detailed studies are required to elucidate the complete signaling pathway. A recent study has localized both EPAC1 and EPAC2 to hair cells in both auditory and vestibular hair cells (51). Only one other study has investigated EPAC in hair cells, where EPAC1 was up-regulated in hair cells following noise exposure and promoted the loss of hair cells (52). Our observations on decreasing gating spring stiffness appear opposite to the effect observed in this study, since decreasing the sensitivity would likely be a protective mechanism to help prevent excitotoxicity of the hair cell. Reconciling these findings may lie in the timescale of effects since our study looked at the effect on the minute timescale, whereas the other study looked at effects on the timescale of days. Nonetheless, these published studies confirm the presence of EPAC in hair cells.

A recent study demonstrated that the diffusivity of the lipid membrane is correlated with the resting P_{open} of the MET channel; manipulations that decrease membrane diffusivity increase the resting P_{open} of the channel (53). Importantly, during a long depolarization (i.e., LDM), the membrane diffusivity increased, suggesting that in the LDM state, membrane diffusivity is increased. It is reasonable to hypothesize that lipid diffusivity may contribute to gating spring stiffness by altering how rigidly the tip link is held in place within the membrane (at either the upper or lower tip-link insertion) or the compliance of the membrane surrounding the channel if MET channels are gated via the lipid membrane itself. Further work is necessary to determine if cAMP/EPAC signaling also increases membrane diffusivity.

In summary, our findings demonstrate that cAMP and long depolarization both modulate the activity of auditory MET by decreasing the stiffness of the gating springs that gate the MET channel. These results demonstrate cAMP regulation of the MET process in mammalian hair cells and introduce a potential mechanism for GPCR regulation of hair cell function.

Methods Summary

Animals were killed using methods approved by the University of Colorado Institutional Animal Care and Use Committee. Patch-clamp electrophysiology, mechanical stimulation, and high-speed imaging of hair bundles are similar to previously described methods on rat cochlear hair cells (18, 19, 24). Iontophoresis was performed using an MVCS 02 (NPI Electronic). Hair bundle stiffness estimates were performed similarly to the methods previously described (26). Data were analyzed using jClamp (SciSoft Company), MATLAB (MathWorks), and Excel (Microsoft). Data are presented as mean ± SD unless otherwise noted. Detailed materials and methods are provided in *SI Appendix, Materials and Methods*.

Data Availability. All data are available upon request by contacting the corresponding author.

ACKNOWLEDGMENTS. We thank Jong-hoon Nam and Gregory Frolenkov for valuable input regarding the work in this manuscript; and Mark Dell'Acqua for steering us toward investigating EPAC-mediated pathways. Initial characterization of LDM was done at Stanford University under support of K99 DC013299 and R01 DC003896. This work was also supported by National Institute on Deafness and Other Communication Disorders Grants R00 DC013299 and R01 DC016868 (to A.W.P.), F31 DC018457 (to A.A.M.), and R21 DC019701 (to G.A.C.).

1. M. Beurg, R. Fettiplace, J. H. Nam, A. J. Ricci, Localization of inner hair cell mechanotransducer channels using high-speed calcium imaging. *Nat. Neurosci.* **12**, 553–558 (2009).
2. B. Pan *et al.*, TMC1 forms the pore of mechanosensory transduction channels in vertebrate inner ear hair cells. *Neuron* **99**, 736–753.e6 (2018).
3. C. L. Cunningham *et al.*, TMIE defines pore and gating properties of the mechanotransduction channel of mammalian cochlear hair cells. *Neuron* **107**, 126–143.e8 (2020).
4. M. Beurg, W. Xiong, B. Zhao, U. Müller, R. Fettiplace, Subunit determination of the conductance of hair-cell mechanotransducer channels. *Proc. Natl. Acad. Sci. U.S.A.* **112**, 1589–1594 (2015).

5. J. Howard, A. J. Hudspeth, Mechanical relaxation of the hair bundle mediates adaptation in mechanoelectrical transduction by the bullfrog's saccular hair cell. *Proc. Natl. Acad. Sci. U.S.A.* **84**, 3064–3068 (1987).
6. J. Howard, A. J. Hudspeth, Compliance of the hair bundle associated with gating of mechanoelectrical transduction channels in the bullfrog's saccular hair cell. *Neuron* **1**, 189–199 (1988).
7. J. O. Pickles, S. D. Comis, M. P. Osborne, Cross-links between stereocilia in the guinea pig organ of Corti, and their possible relation to sensory transduction. *Hear. Res.* **15**, 103–112 (1984).
8. J. A. Assad, G. M. Shepherd, D. P. Corey, Tip-link integrity and mechanical transduction in vertebrate hair cells. *Neuron* **7**, 985–994 (1991).
9. S. Li *et al.*, Myosin-VIIa is expressed in multiple isoforms and essential for tensioning the hair cell mechanotransduction complex. *Nat. Commun.* **11**, 2066 (2020).
10. S. L. Shotwell, R. Jacobs, A. J. Hudspeth, Directional sensitivity of individual vertebrate hair cells to controlled deflection of their hair bundles. *Ann. N. Y. Acad. Sci.* **374**, 1–10 (1981).
11. R. A. Eatock, D. P. Corey, A. J. Hudspeth, Adaptation of mechanoelectrical transduction in hair cells of the bullfrog's sacculus. *J. Neurosci.* **7**, 2821–2836 (1987).
12. A. J. Ricci, H. J. Kennedy, A. C. Crawford, R. Fettiplace, The transduction channel filter in auditory hair cells. *J. Neurosci.* **25**, 7831–7839 (2005).
13. H. J. Kennedy, A. C. Crawford, R. Fettiplace, Force generation by mammalian hair bundles supports a role in cochlear amplification. *Nature* **433**, 880–883 (2005).
14. A. W. Peng, F. T. Salles, B. Pan, A. J. Ricci, Integrating the biophysical and molecular mechanisms of auditory hair cell mechanotransduction. *Nat. Commun.* **2**, 523 (2011).
15. A. J. Ricci, R. Fettiplace, The effects of calcium buffering and cyclic AMP on mechano-electrical transduction in turtle auditory hair cells. *J. Physiol.* **501**, 111–124 (1997).
16. P. Martin, D. Bozovic, Y. Choe, A. J. Hudspeth, Spontaneous oscillation by hair bundles of the bullfrog's sacculus. *J. Neurosci.* **23**, 4533–4548 (2003).
17. R. L. Santos-Cortez *et al.*; University of Washington Center for Mendelian Genomics, Adenylate cyclase 1 (ADCY1) mutations cause recessive hearing impairment in humans and defects in hair cell function and hearing in zebrafish. *Hum. Mol. Genet.* **23**, 3289–3298 (2014).
18. G. A. Caprara, A. A. Mecca, A. W. Peng, Decades-old model of slow adaptation in sensory hair cells is not supported in mammals. *Sci. Adv.* **6**, eabb4922 (2020).
19. G. A. Caprara, A. A. Mecca, Y. Wang, A. J. Ricci, A. W. Peng, Hair bundle stimulation mode modifies manifestations of mechanotransduction adaptation. *J. Neurosci.* **39**, 9098–9106 (2019).
20. H. Kumagami *et al.*, Expression pattern of adenylyl cyclase isoforms in the inner ear of the rat by RT-PCR and immunochemical localization of calcineurin in the organ of Corti. *Hear. Res.* **132**, 69–75 (1999).
21. M. J. Drescher *et al.*, Expression of adenylyl cyclase type I in cochlear inner hair cells. *Brain Res. Mol. Brain Res.* **45**, 325–330 (1997).
22. N. Michalski *et al.*, Molecular characterization of the ankle-link complex in cochlear hair cells and its role in the hair bundle functioning. *J. Neurosci.* **27**, 6478–6488 (2007).
23. A. W. Peng, T. Effertz, A. J. Ricci, Adaptation of mammalian auditory hair cell mechanotransduction is independent of calcium entry. *Neuron* **80**, 960–972 (2013).
24. A. W. Peng, R. Gnanasambandam, F. Sachs, A. J. Ricci, Adaptation independent modulation of auditory hair cell mechanotransduction channel open probability implicates a role for the lipid bilayer. *J. Neurosci.* **36**, 2945–2956 (2016).
25. S. Kitajiri *et al.*, Actin-bundling protein TRIOBP forms resilient rootlets of hair cell stereocilia essential for hearing. *Cell* **141**, 786–798 (2010).
26. M. Tobin, A. Chaiyasitdhi, V. Michel, N. Michalski, P. Martin, Stiffness and tension gradients of the hair cell's tip-link complex in the mammalian cochlea. *eLife* **8**, e43473 (2019).
27. M. Beurg, J. H. Nam, A. Crawford, R. Fettiplace, The actions of calcium on hair bundle mechanics in mammalian cochlear hair cells. *Biophys. J.* **94**, 2639–2653 (2008).
28. F. Jaramillo, A. J. Hudspeth, Displacement-clamp measurement of the forces exerted by gating springs in the hair bundle. *Proc. Natl. Acad. Sci. U.S.A.* **90**, 1330–1334 (1993).
29. C. Liu, P. Ke, J. Zhang, X. Zhang, X. Chen, Protein kinase inhibitor peptide as a tool to specifically inhibit protein kinase A. *Front. Physiol.* **11**, 574030 (2020).
30. T. Chijiwa *et al.*, Inhibition of forskolin-induced neurite outgrowth and protein phosphorylation by a newly synthesized selective inhibitor of cyclic AMP-dependent protein kinase, N-[2-(p-bromocinnamylamino)ethyl]-5-isoquinolinesulfonamide (H-89), of PC12D pheochromocytoma cells. *J. Biol. Chem.* **265**, 5267–5272 (1990).
31. D. J. Jagger, J. F. Ashmore, The fast activating potassium current, I(K,f), in guinea-pig inner hair cells is regulated by protein kinase A. *Neurosci. Lett.* **263**, 145–148 (1999).
32. J. de Rooij *et al.*, Epac is a Rap1 guanine-nucleotide-exchange factor directly activated by cyclic AMP. *Nature* **396**, 474–477 (1998).
33. M. Schmidt, F. J. Dekker, H. Maarsingh, Exchange protein directly activated by cAMP (epac): A multidomain cAMP mediator in the regulation of diverse biological functions. *Pharmacol. Rev.* **65**, 670–709 (2013).
34. J. M. Enserink *et al.*, A novel Epac-specific cAMP analogue demonstrates independent regulation of Rap1 and ERK. *Nat. Cell Biol.* **4**, 901–906 (2002).
35. H. Rehmann, F. Schwede, S. O. Døskeland, A. Wittinghofer, J. L. Bos, Ligand-mediated activation of the cAMP-responsive guanine nucleotide exchange factor Epac. *J. Biol. Chem.* **278**, 38548–38556 (2003).
36. G. A. Caprara, A. W. Peng, Mechanotransduction in mammalian sensory hair cells. *Mol. Cell. Neurosci.* **120**, 103706 (2022).
37. H. Rehmann, Epac-inhibitors: Facts and artefacts. *Sci. Rep.* **3**, 3032 (2013).
38. R. J. de Wit *et al.*, Inhibitory action of certain cyclophosphate derivatives of cAMP on cAMP-dependent protein kinases. *Eur. J. Biochem.* **142**, 255–260 (1984).
39. B. Kachar, M. Parakkal, M. Kurc, Y. Zhao, P. G. Gillespie, High-resolution structure of hair-cell tip links. *Proc. Natl. Acad. Sci. U.S.A.* **97**, 13336–13341 (2000).
40. M. Sotomayor, W. A. Weihofen, R. Gaudet, D. P. Corey, Structural determinants of cadherin-23 function in hearing and deafness. *Neuron* **66**, 85–100 (2010).
41. T. F. Bartsch *et al.*, Elasticity of individual protocadherin 15 molecules implicates tip links as the gating springs for hearing. *Proc. Natl. Acad. Sci. U.S.A.* **116**, 11048–11056 (2019).
42. G. Dionne *et al.*, Mechanotransduction by PCDH15 relies on a novel *cis*-dimeric architecture. *Neuron* **99**, 480–492.e5 (2018).
43. M. Grati, B. Kachar, Myosin VIIa and sans localization at stereocilia upper tip-link density implicates these Usher syndrome proteins in mechanotransduction. *Proc. Natl. Acad. Sci. U.S.A.* **108**, 11476–11481 (2011).
44. N. Grillet *et al.*, Harmonin mutations cause mechanotransduction defects in cochlear hair cells. *Neuron* **62**, 375–387 (2009).
45. W. Xiong *et al.*, TMHS is an integral component of the mechanotransduction machinery of cochlear hair cells. *Cell* **151**, 1283–1295 (2012).
46. B. Zhao *et al.*, TMIE is an essential component of the mechanotransduction machinery of cochlear hair cells. *Neuron* **84**, 954–967 (2014).
47. B. Pan *et al.*, TMC1 and TMC2 are components of the mechanotransduction channel in hair cells of the mammalian inner ear. *Neuron* **79**, 504–515 (2013).
48. A. P. J. Giese *et al.*, CIB2 interacts with TMC1 and TMC2 and is essential for mechanotransduction in auditory hair cells. *Nat. Commun.* **8**, 43 (2017).
49. R. J. Powers *et al.*, Stereocilia membrane deformation: Implications for the gating spring and mechanotransduction channel. *Biophys. J.* **102**, 201–210 (2012).
50. B. J. Zieba *et al.*, The cAMP-responsive Rap1 guanine nucleotide exchange factor, Epac, induces smooth muscle relaxation by down-regulation of RhoA activity. *J. Biol. Chem.* **286**, 16681–16692 (2011).
51. C. Wang *et al.*, The expression and significance of Epac1 and Epac2 in the inner ear of guinea pigs. *Eur. Arch. Otorhinolaryngol.*, 10.1007/s00405-022-07380-0 (2022).
52. F. Sun *et al.*, Epac1 signaling pathway mediates the damage and apoptosis of inner ear hair cells after noise exposure in a rat model. *Neuroscience* **465**, 116–127 (2021).
53. S. S. George, C. R. Steele, A. J. Ricci, Rat auditory inner hair cell mechanotransduction and stereociliary membrane diffusivity are similarly modulated by calcium. *iScience* **23**, 101773 (2020).